Inhomogeneous fluids of colloidal hard dumbbells: Fundamental measure theory and Monte Carlo simulations

Matthieu Marechal, Hanns Hagen Goetzke, Andreas Härtel, and Hartmut Löwen

Citation: J. Chem. Phys. **135**, 234510 (2011); doi: 10.1063/1.3664742
View online: http://dx.doi.org/10.1063/1.3664742
View Table of Contents: http://jcp.aip.org/resource/1/JCPSA6/v135/i23
Published by the American Institute of Physics.

Inhomogeneous fluids of colloidal hard dumbbells: Fundamental measure theory and Monte Carlo simulations

Matthieu Marechal, Hanns Hagen Goetzke, Andreas Härtel, and Hartmut Löwen[a)]
Institut für Theoretische Physik II, Heinrich-Heine Universität Düsseldorf, Universitätsstraße 1, 40225 Düsseldorf, Germany

(Received 22 September 2011; accepted 8 November 2011; published online 19 December 2011)

Recently, a density functional theory for hard particles with shape anisotropy was developed, the extended deconvolution fundamental measure theory (edFMT). We apply edFMT to hard dumbbells, arguably the simplest non-convex shape and readily available experimentally in the form of colloids. We obtain good agreement between edFMT and Monte Carlo simulations for fluids of dumbbells in a slit and for the same system under gravity. This indicates that edFMT can be successfully applied to nearly all colloidal shapes, not just for the convex shapes for which edFMT was originally derived. A theory, such as edFMT, that allows a fast and general way of mapping the phase behavior of anisotropic colloids, can act as a useful guide for the design of colloidal shapes for various applications. © *2011 American Institute of Physics*. [doi:10.1063/1.3664742]

I. INTRODUCTION

Density functional theory (DFT) (Refs. 1 and 2) is naturally applicable whenever the density profile is inhomogeneous, such as under applied external fields[1,3,4] and in the case of bulk freezing.[5–7] Hard spheres represent a classical and quite tractable system to which density functional theory has been applied in many studies. One of the most successful versions of DFT for hard spheres is fundamental measure theory (FMT), which is based on the fundamental measures of a sphere, its radius, area and volume.[8] A version of FMT derived from the 0-dimensional limit[9,10] has proven to be very successful in predicting the properties of the crystal.[6] This FMT has been further modified to yield the excellent Carnahan-Starling equation of state[11] for the homogeneous fluid, and the resulting FMT predicts the hard sphere freezing transition very accurately.[12,13]

Simultaneously, the interest in liquid crystals has been a motivation to apply DFT to anisotropic particles, for instance, hard spherocylinders, idealized rod-like molecules. The isotropic–smectic and nematic–smectic phase transitions of these rods were determined using a weighted density version of DFT for anisotropic particles[14,15] and showed reasonable agreement with the essentially exact simulations results of Ref. 16. However, the construction of the free energy functional of this theory is ad hoc and we would like to use a functional based solely on the geometry of the particles. Such density functional theories have been constructed for specific shapes with zero volume, namely infinitely thin rods[17] and disks.[18]

Rosenfeld extended his version of FMT for spheres to general anisotropic particle shapes.[19] However, this version did not predict a stable nematic phase for any particle-shape. This deficiency was repaired recently by Hansen-Goos and Mecke,[3,4] who derived the so-called extended deconvolution FMT (edFMT) from the low-density limit in a more precise manner. The resulting isotropic-nematic transition shows excellent agreement with simulations.[4,20] In another recent study, the theory has been applied to fluids of spherocylinders under the influence of an external field that couples to the orientations of the particles and a dynamic version of edFMT has been derived for time dependent external fields.[20,21]

Although a version of FMT has been proposed for spherically symmetric soft interactions,[22,23] it is not as successful as the fundamental measure theories for hard particles. Historically, hard-core interaction potentials have been very useful as the basis for theories that apply to more general atomic and molecular systems. More recently, the realization of hard-particle systems in the form of colloidal suspensions has given the study of anisotropic hard particles a new incentive. Colloids have been synthesized in an impressive number of shapes,[24] many of which have no atomic or molecular analogue. Many of these colloidal shapes are non-convex and a theory predicting the phase behavior of non-convex particles would be of great value. Although convexity of the particle-shape is assumed in their derivations and so far only convex shapes have been studied, the recent edFMT[4] and the older version of FMT[19] for anisotropic particles are expected to approximately hold for non-convex particles as well. The primary goal of this paper is to test this expectation by investigating the accuracy of edFMT for non-convex particles.

Dumbbells, that consist of two fused hard spheres, are arguably the simplest non-convex colloids. A reason for investigating this model, apart from its simplicity, is that colloids with the exact shape of the dumbbell can be fairly easily synthesized. In fact, quite a few different synthesis methods have been successfully applied.[25–27] Colloidal dumbbells have been used to experimentally investigate bulk crystallization,[28] quasi-two-dimensional degenerate crystals[27,29,30] and the effects of charge and an external electric field on a bulk crystal.[31] Furthermore, the phase behavior of bulk systems of the dumbbells is well-known from simulations,[32–36] which is convenient for further studies.

[a)]Electronic mail: hlowen@thphy.uni-duesseldorf.de.

Wall effects and effects of gravity are typically very important in colloidal suspensions, which can be exploited to steer crystallization, for instance by sedimentation onto a substrate.[37–39] Therefore, it is paramount to investigate the effects of gravity and of the confining walls on colloidal suspensions. Simulation studies on crystallization of spheres,[40,41] spherocylinders[42] and dumbbells[43] have shown that the phase behavior of the system under gravity can be understood by a mapping onto the bulk phase diagram. Comparisons between the density profiles for fluids in the presence of external fields obtained from DFT calculations and those measured in simulations are often used to validate the theoretical approach. For instance, the FMT for hard spheres has been very successful in describing the density profile near a hard wall[12] and edFMT is equally successful for (convex) spherocylinders.[3,4] The density profile obtained from an older semi-empirical weighted density approach, specifically tailored to dumbbells, has also shown quite good agreement with simulation results.[44] However, the deviation between the simulations and the semi-empirical DFT for dumbbells[44] is larger than the deviation between results from simulations and edFMT for spherocylinders.[4] In this work, we will compare density profiles of dumbbell fluids in between two walls or under gravity obtained from edFMT to those measured in simulations. We will show that the edFMT performs better than the semi-empirical DFT for dumbbells, but results in somewhat less good agreement with our simulations for the non-convex dumbbells than for the convex spherocylinders.[4]

The paper is organized as follows: First, we will describe the model we use for the dumbbell and define its aspect ratio. Next, the general frame work as derived in Ref. 4 will be summarized. In the following section, we will point out the additional approximation which is made when considering non-convex particles, instead of convex particles. We will also briefly describe the details of the Monte Carlo simulations and define the density and orientational order profiles which we employ. Turning to the results, we will first show the reasonable agreement between edFMT results and simulation data for a dumbbell fluid near a wall when the adjustable parameter ζ in edFMT is set to zero. The merits of using a (semi-empirical) nonzero value for ζ are discussed next. The effect of wall spacing on the density profile of a fluid in confinement is also shown. The effects of applying a gravitational field are briefly discussed and, finally, we present some conclusions.

II. MODEL AND SYSTEM PARAMETERS

We consider a system of hard dumbbells consisting of spheres of diameter σ whose centers are separated by a distance $L \leq \sigma$. Accordingly, $L^* \equiv L/\sigma = 0$ corresponds to a single sphere, while the dumbbell consists of the touching spheres for $L^* = 1$. In Fig. 1, the dimensions L and σ of a dumbbell are indicated. Three values for $L^* = 0.3$, 0.6, and 0.9 will be considered in this work; the shape of the corresponding dumbbells varies from basically convex and similar to a spherocylinder for $L^* = 0.3$, to highly non-convex for $L^* = 0.9$. We have briefly investigated a few other values of L^* and found no qualitative differences. We will consider systems which are inhomogeneous due to the presence of an external potential resulting either from a gravitational field and a hard bottom wall or from two hard walls. Only densities or chemical potentials below the crystallization transition[36,43] will be considered, such that the system is fluid-like at all heights. The direction of gravity and the normals to the walls are along the z-direction. When the external potential is only due to two hard walls, the averaged packing fraction $\eta = v_{\rm db}N/(HA)$ is fixed, where N is the number of particles, $v_{\rm db} = \frac{\pi}{6}(\sigma^3 + \frac{3}{2}L\sigma^2 - \frac{1}{2}L^3)$ is the volume of a dumbbell, H is the distance between the walls and A is the area of the system perpendicular to the z direction. The chemical potential μ is held fixed when the system is subjected to a gravitational field (η is then zero because the system extends up to infinity in the positive z-direction). The dimensionless chemical potential μ^* is defined as $\mu^* = \beta[\mu - \log(\mathcal{V}/4\pi\sigma^3)]$, where $\mathcal{V}$ is the thermal volume and $\beta = 1/k_BT$ (k_B is Boltzmann's constant and T the temperature). The shift $-\log(\mathcal{V}/\sigma^3)$ removes the terms in the chemical potential that result from the integrals over the translational and angular momenta in the partition sum. The value of the thermal volume has no effect on velocity-independent properties in equilibrium, such as the ones investigated here. The dimensionless strength of the gravitational field is defined as $g^* = mg\sigma/k_BT$, where m is the (buoyant) mass of the dumbbell and g is the gravitational acceleration. The definitions of μ^* and g^* are such that the density $\rho(z)$ at large height z is given by $\lim_{z\to\infty}\rho(z)\sigma^3 = \exp(\mu^* - g^*z/\sigma)$, a dimensionless form of the barometric formula.

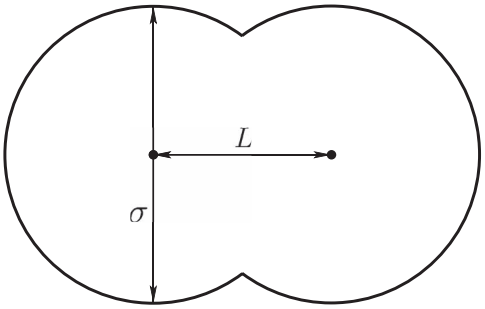

FIG. 1. The dimensions of a dumbbell: the diameter σ of its constituent spheres and the distance L between the centers of the spheres. The aspect ratio is defined as $L^* \equiv L/\sigma$.

III. METHODS

A. Theory

Density functional theory is based on the exact result that the density profile can be obtained by minimizing an expression of the form[1]

$$\Omega[\rho] = \mathcal{F}_{\rm int}[\rho] + \sum_\nu \int \rho_\nu(\mathbf{r})(V_\nu^{\rm ext}(\mathbf{r}) - \mu_\nu)d\mathbf{r}, \qquad (1)$$

with respect to the density profile $\rho_\nu(\mathbf{r})$ itself, where μ_ν is the chemical potential of species/orientation ν ($\mu_o = \mu_\nu$ for all o that denote rotated copies of ν), $V_\nu^{\rm ext}$ is the external potential experienced by a particle of species/orientation ν at posi-

tion **r**. We will use the notation of Ref. 19, where ν denotes a specific shape, size, and orientation for brevity. Accordingly, the sum over ν denotes a sum over all species and, for each anisotropic species, an integral over its orientations. We will only consider one-component systems in this work, but write down the general framework of edFMT for the more general case of mixtures of anisotropic particles. The functional $\mathcal{F}_{\rm int}[\rho]$ is independent of $V_\nu^{\rm ext}(\mathbf{r})$, allowing reliable approximations based solely on the bulk phase behavior. We will first describe the extended deconvolution fundamental measure theory (edFMT),[3,4] for general particle shapes and subsequently apply it to dumbbells.

1. General framework of fundamental measure theory

The bulk free energy of edFMT is[3,4]

$$\mathcal{F}_{\rm int} = \mathcal{F}_{\rm id} + \mathcal{F}_{\rm exc} = k_B T \int (\Phi_{\rm id} + \Phi_{\rm exc}) \mathrm{d}\mathbf{r}, \tag{2}$$

where $\Phi_{\rm id} = \sum_\nu \rho_\nu \log(\rho_\nu \mathcal{V}) - \rho_\nu$ and

$$\begin{aligned}\Phi_{\rm exc} = &-n_0 \log(1-n_3) \\ &+ \frac{n_1 n_2 - \vec{n}_1 \cdot \vec{n}_2 - \zeta \overleftrightarrow{n}_1 : \overleftrightarrow{n}_2}{1-n_3} \\ &+ \frac{3}{16\pi} \frac{\vec{n}_2 \cdot \overleftrightarrow{n}_2 \cdot \vec{n}_2 - n_2 |\vec{n}_2|^2 - \mathrm{Tr}[\overleftrightarrow{n}_2{}^3] + n_2 \overleftrightarrow{n}_2 : \overleftrightarrow{n}_2}{(1-n_3)^2},\end{aligned} \tag{3}$$

with $\mathrm{Tr}[A]$ equal to the trace of a matrix A and $A:B \equiv \mathrm{Tr}[AB]$. While the ideal gas part of the free energy density $\Phi_{\rm id}$ is a function of the local one-body density $\rho(\mathbf{r})$ at position **r**, the excess free energy density $\Phi_{\rm exc}(\{n_\alpha[\rho](\mathbf{r})\})$, depends only on the weighted densities

$$n_\alpha(\mathbf{r}) \equiv \sum_\nu \int \rho_\nu(\mathbf{r}') w_\nu^{(\alpha)}(\mathbf{r}-\mathbf{r}') \mathrm{d}\mathbf{r}', \tag{4}$$

where $w_\nu^{(\alpha)}(\mathbf{r})$ are the weight functions of species/orientation ν. The set $\{w^{(\alpha)}(\mathbf{r})\}$ consists of four scalar weight functions,

$$w_\nu^{(3)}(\mathbf{r}) = \Theta(|\mathbf{r}| - R_\nu(\hat{r})), \tag{5}$$

$$w_\nu^{(2)}(\mathbf{r}) = \frac{1}{\mathbf{n}(\hat{r})\cdot\hat{r}} \delta(|\mathbf{r}| - R_\nu(\hat{r})), \tag{6}$$

$$w_\nu^{(1)}(\mathbf{r}) = \frac{H_\nu(\hat{r})}{4\pi} w_\nu^{(2)}(\mathbf{r}), \tag{7}$$

$$w_\nu^{(0)}(\mathbf{r}) = \frac{K_\nu(\hat{r})}{4\pi} w_\nu^{(2)}(\mathbf{r}), \tag{8}$$

two vectorial weight functions,

$$\vec{w}_\nu^{(2)}(\mathbf{r}) = \mathbf{n}_\nu(\hat{r}) w_\nu^{(2)}(\mathbf{r}), \tag{9}$$

$$\vec{w}_\nu^{(1)}(\mathbf{r}) = \mathbf{n}_\nu(\hat{r}) w_\nu^{(1)}(\mathbf{r}), \tag{10}$$

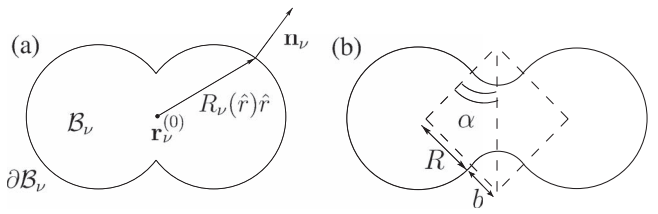

FIG. 2. (a) The surface $\partial\mathcal{B}_\nu$ of a body $\mathcal{B}_\nu$ is parametrized by a unit vector $\hat{r}$, such that the corresponding point on the surface is $R_\nu(\hat{r})\hat{r}$. The normal at this point is denoted by $\mathbf{n}_\nu(\hat{r})$. (b) The kink in the surface of a dumbbell is regularized by replacing it by a section of a torus, as indicated by the small arcs. The torus has a tube radius of b and the dumbbell is recovered in the limit $b \to 0$.

and two tensorial weight functions of rank two,

$$\begin{aligned}\overleftrightarrow{w}_\nu^{(2)}(\mathbf{r}) &= \mathbf{n}_\nu(\hat{r})\mathbf{n}_\nu(\hat{r})^T \\ \overleftrightarrow{w}_\nu^{(1)}(\mathbf{r}) &= \frac{\Delta\kappa_\nu(\hat{r})}{4\pi} \\ &\quad \times \left[\mathbf{v}_\nu^I(\hat{r})\mathbf{v}_\nu^I(\hat{r})^T - \mathbf{v}_\nu^{II}(\hat{r})\mathbf{v}_\nu^{II}(\hat{r})^T\right] w_\nu^{(2)}(\mathbf{r}).\end{aligned} \tag{11}$$

Here, the unit vector $\hat{r} = \mathbf{r}/|\mathbf{r}|$, $R_\nu(\hat{r})$ is the distance along $\hat{r}$ from a conveniently chosen point $\mathbf{r}_\nu^{(0)}$ inside the volume of the particle ν to the surface and $\mathbf{n}_\nu(\hat{r})$ is the normal to the surface at $R_\nu(\hat{r})\hat{r}$, see Fig. 2(a). Moreover, $K_\nu(\hat{r}) = \kappa_\nu^I(\hat{r})\kappa_\nu^{II}(\hat{r})$ denotes the Gaussian curvature, $H_\nu(\hat{r}) = \frac{1}{2}(\kappa_\nu^I(\hat{r}) + \kappa_\nu^{II}(\hat{r}))$ is the mean curvature and $\Delta\kappa_\nu(\hat{r}) = \frac{1}{2}(\kappa_\nu^I(\hat{r}) - \kappa_\nu^{II}(\hat{r}))$ denotes the deviatoric curvature, where $\kappa_\nu^I(\hat{r})$ and $\kappa_\nu^{II}(\hat{r})$ are the principal moments of the curvature in the directions $\mathbf{v}^I(\hat{r})$ and $\mathbf{v}^{II}(\hat{r})$, respectively, at the point $R_\nu(\hat{r})\hat{r}$ on the surface of the body ν, see Fig. 2. We show that the free energy functional (2) can also be derived from the zero-dimensional limit in Appendix B.

Hansen-Goos and Mecke[3,4] derived an expansion of the Mayer function $f_{\nu o}(\mathbf{r}_o - \mathbf{r}_\nu)$, which is -1 upon overlap of bodies ν and o and zero otherwise, in terms of ever higher rank tensorial weight functions. The parameter ζ is a renormalization factor introduced by Hansen-Goos and Mecke[3,4] to correct for the truncation of this expansion of the Mayer function after the term involving rank two tensors. The factor ζ should be independently determined for every particle shape by minimizing the mean squared difference between the exact excluded volume $v_{\nu,o}^{\rm excl}$ and the edFMT approximation $v_{\nu,o}^{\rm edFMT}$, where the excluded volume is given by

$$v_{\nu,o}^{\rm excl} = -\frac{1}{V}\int_V \int_V f_{\nu o}(\mathbf{r}_\nu - \mathbf{r}_o) \mathrm{d}\mathbf{r}_\nu \mathrm{d}\mathbf{r}_o, \tag{12}$$

and the edFMT approximation, $v_{\nu,o}^{\rm edFMT}$, is obtained in the same way with $f_{\nu o}(\mathbf{r}_\nu - \mathbf{r}_o)$ replaced by the approximated Mayer function $f_{\nu o}^{\rm edFMT}(\mathbf{r}_\nu - \mathbf{r}_o)$, which depends on ζ. The structure of very elongated particles is determined to a large degree by the excluded volume, which justifies its use for determining ζ for the spherocylinders with total-length-over-diameter ratio larger than 3.5 to which edFMT was applied in Refs. 3, 4, 20, and 21. For less elongated particles, the excluded volume is not the only important quantity as the

structure is determined by both translational and positional ordering. Therefore, it is somewhat arbitrary to fit ζ by minimizing the difference between the exact and edFMT excluded volumes. Furthermore, other approximations are made than the truncation of the tensor-expansion at first order when edFMT is applied to non-convex particles, as described in the next section. We will show that the most pronounced effects of these additional approximations can not be decreased by choosing an appropriate value for ζ. Therefore, we set ζ to zero unless indicated otherwise. We will show that edFMT still yields reasonable results for inhomogeneous fluids of dumbbells even with $\zeta = 0$.

2. Effect of the non-convexity

In this subsection, we will explicitly write down the difficulties arising when edFMT is applied to non-convex particles. In the Results section, we will show that edFMT is still a surprisingly good density functional theory, in spite of these difficulties.

A crucial part of the derivation of the free energy (2) in Ref. 4 is to express the Mayer function $f_{vo}(\mathbf{r}_v - \mathbf{r}_o)$ in terms of the weight functions listed above by a deconvolution. This deconvolution is performed with the aid of the Gauss-Bonnet theorem,[45] which reads

$$\int_S K \,\mathrm{d}A + \int_{\partial S} \kappa_g \mathrm{d}s = 2\pi\,\chi(S), \tag{13}$$

where S is a compact surface, K is the Gaussian curvature and κ_g the geodesic curvature along the edge ∂S of surface S. The Euler characteristic $\chi(S)$ describes the topology of S; the $\chi(S)$ values of the shapes relevant for this work will be mentioned as we encounter them. In the case of two intersecting *convex* particles, it is easy to show that the intersection $\mathcal{B}_v \cap \mathcal{B}_o$ is again a convex body, which has an Euler characteristic of two (it is topologically equivalent to the surface of a sphere). If $\mathcal{B}_v$ and $\mathcal{B}_o$ do not overlap $\chi(\partial[\mathcal{B}_v \cap \mathcal{B}_o])$ is equal to the Euler characteristic of the empty set, which is zero. In other words, the Mayer function f_{vo} is equal to $-\chi(\partial[\mathcal{B}_v \cap \mathcal{B}_o])/2$ for convex $\mathcal{B}_v$ and $\mathcal{B}_o$. The surface of the intersection consists of two parts: $\partial\mathcal{B}_v \cap \mathcal{B}_o$, the part of the surface of B_v in B_o, and $\mathcal{B}_v \cap \partial\mathcal{B}_o$. For the type of surfaces we are interested in, the Euler characteristic of a union is equal to $\chi(A \cup B) = \chi(A) + \chi(B) - \chi(A \cap B)$. Consequently,

$$\begin{aligned}\chi(\partial[\mathcal{B}_v \cap \mathcal{B}_o]) &= \chi(\partial\mathcal{B}_v \cap \mathcal{B}_o) + \chi(\mathcal{B}_v \cap \partial\mathcal{B}_o) - \chi(\partial\mathcal{B}_v \cap \partial\mathcal{B}_o) \\ &= \chi(\partial\mathcal{B}_v \cap \mathcal{B}_o) + \chi(\mathcal{B}_v \cap \partial\mathcal{B}_o),\end{aligned} \tag{14}$$

where the last equality holds because $\partial\mathcal{B}_v \cap \partial\mathcal{B}_o$ consists of one or more loops, with Euler characteristic zero. Consequently, the Gauss-Bonnet theorem, with $S = \partial\mathcal{B}_v \cap \mathcal{B}_o$ and $\mathcal{B}_v \cap \partial\mathcal{B}_o$ can be used to write the Mayer function, written as $-\chi(\partial[\mathcal{B}_v \cap \mathcal{B}_o])/2$, in terms of the integrals on the left hand side of (13). These integrals can be expressed in terms of the weighted density functions of Eqs. (5)–(11) plus terms involving tensors of rank higher than two, see Ref. 4. Again, these higher rank tensors are ignored in most of Ref. 4, and in the whole of this work.

The intersection of two *non*-convex particles is not always a single, convex body.[46] For example, the intersection between two dumbbells can consist of n disjoint convex bodies for $n = 1, 2, 3, 4$, with $\chi(\partial[\mathcal{B}_v \cap \mathcal{B}_o]) = 2n$ and it can also be a single body with a hole in it, leading to $\chi(\partial[\mathcal{B}_v \cap \mathcal{B}_o]) = 0$. So setting the Mayer function equal to $-\chi(\partial[\mathcal{B}_v \cap \mathcal{B}_o])/2$, as is done in edFMT, is an approximation for non-convex particles. However, this is not a bad approximation as long as the intersection between the particles in most of the possible configurations is a single simply connected body (i.e., without any holes) with Euler characteristic two.

Finally, the deconvolution of the Mayer function in terms of weight functions can be used to derive Eq. (2) using methods developed by Rosenfeld[8] and Tarazona.[6,10] This procedure is described in sufficient detail in Ref. 4 and we will not repeat this derivation here.

Finally, we note that the definition of surface in terms of the distance $R_v(\hat{r})$ from the surface to the reference point $\mathbf{r}_v^{(0)}$ along a ray $\hat{r}$ is ambiguous for some non-convex particles, as some rays may cross the surface of the particle in more than one point. In this case, the weighted densities can no longer be written as the convolution (4), and should be defined as

$$n_\alpha(\mathbf{r}) \equiv \sum_v \begin{cases} \int_{\mathcal{B}_v} \rho_v(\mathbf{r} - \mathbf{r}')\mathrm{d}\mathbf{r}' & \alpha = 3, \\ \int_{\partial\mathcal{B}_v} \rho_v(\mathbf{r} - \mathbf{R}_v(\mathbf{s}))\bar{w}_v^{(\alpha)}(\mathbf{s})\mathrm{d}^2\mathbf{s} & \text{otherwise,} \end{cases} \tag{15}$$

where $\mathcal{B}_v$ is the particle of species/orientation v, while $\partial\mathcal{B}_v$ is its surface, parametrized by $\mathbf{s}$ and with surface element $\mathrm{d}^2\mathbf{s}$. Furthermore, the function $\bar{w}_v^{(\alpha)}(\mathbf{s})$ denotes the weight functions $w_v^{(\alpha)}$ for $\alpha \neq 3$ as listed above with the factor $w_v^{(2)}$ removed ($\bar{w}_v^{(2)}(\mathbf{s}) = 1$). The weighted densities are also written in this form in this work—although this is not necessary for dumbbells—because it leads to simpler expressions for the weight functions.

3. Application to dumbbells

We will now consider one-component systems of dumbbells. Accordingly, we replace the sum over v by $\int \mathrm{d}\mathbf{u}$, where $\mathbf{u}$ is the orientation of a dumbbell, such that the density profile becomes $\rho(\mathbf{r}, \mathbf{u})$. For dumbbells, a difficulty arises in evaluating the weight function at the "neck" of the dumbbell, i.e., the intersection circle between the partial spherical shells that the surface of the dumbbell consists of, since the curvature on this circle is ill-defined. To circumvent this problem, we redefine the dumbbell as the limit of a particle with a smooth surface for which the "neck" is replaced by some inner section of a torus, see Fig. 2(b). After performing this limit, the scalar, vector and tensor weighted densities $n_\alpha(\mathbf{r})$ for $\alpha = 0$, 1, 2 can be expressed as

$$\begin{aligned}&\int \sum_{m=+,-} \int_{S_m(\mathbf{u})} R^2\, \bar{w}_h^{(\alpha)}(\mathbf{s}, \mathbf{u}) \rho\left(\mathbf{r} - m\frac{L}{2}\mathbf{u} - R\mathbf{s}, \mathbf{u}\right) \mathrm{d}^2\mathbf{s} \\ &\quad + \int_{C(\mathbf{u})} \bar{w}_c^{(\alpha)}(l, \mathbf{u}) \rho(\mathbf{r} - R_c\mathbf{n}_c(l, \mathbf{u}), \mathbf{u}) \mathrm{d}l\, \mathrm{d}\mathbf{u},\end{aligned} \tag{16}$$

where $S_m(\mathbf{u})$ consist of all $\mathbf{s}$ on the unit sphere, such that $m\mathbf{s} \cdot \mathbf{u} > -L/\sigma$, $C(\mathbf{u})$ is the circle where the curvature has a singularity, l parametrizes $C(\mathbf{u})$, $R_c \equiv \sqrt{R^2 - L^2/4}$ is the

radius of $C(\mathbf{u})$ and $\mathbf{n}_c(l)$ is the normal to this circle in the plane perpendicular to $\mathbf{u}$. The functions $\bar{w}_h^{(\alpha)}$, that are integrated over one half of the surface of a dumbbell in Eq. (16), are

$$\bar{w}_h^{(0)}(\mathbf{s},\mathbf{u}) = 1/(4\pi R^2), \tag{17}$$

$$\bar{w}_h^{(1)}(\mathbf{s},\mathbf{u}) = 1/(4\pi R), \quad \bar{w}_h^{(2)}(\mathbf{s},\mathbf{u}) = 1, \tag{18}$$

$$\vec{\bar{w}}_h^{(1)}(\mathbf{s},\mathbf{u}) = \mathbf{s}/(4\pi R), \quad \vec{\bar{w}}_h^{(2)}(\mathbf{s},\mathbf{u}) = \mathbf{s}, \tag{19}$$

$$\overleftrightarrow{\bar{w}}_h^{(1)}(\mathbf{s},\mathbf{u}) = \overleftrightarrow{0}, \quad \overleftrightarrow{\bar{w}}_h^{(2)}(\mathbf{s},\mathbf{u}) = \mathbf{s}\,\mathbf{s}^T, \tag{20}$$

which are just the weight functions of a sphere, while the functions $\bar{w}_c^{(\alpha)}$, that are integrated over the "neck" of the dumbbell, are given by

$$\bar{w}_c^{(0)}(l,\mathbf{u}) = -L^*/(2\pi R_c), \tag{21}$$

$$\bar{w}_c^{(1)}(l,\mathbf{u}) = -\alpha_0/(4\pi), \tag{22}$$

$$\bar{w}_c^{(2)}(l,\mathbf{u}) = 0, \tag{23}$$

$$\vec{\bar{w}}_c^{(1)}(l,\mathbf{u}) = -\mathbf{n}_c(l)L^*/(4\pi) \tag{24}$$

$$\vec{\bar{w}}_c^{(2)}(l,\mathbf{u}) = 0 \tag{25}$$

$$\overleftrightarrow{\bar{w}}_c^{(1)}(l,\mathbf{u}) = \frac{1}{4\pi}\left[\alpha_0\mathbb{I} - \left(\frac{3}{2}\alpha_0 + \frac{1}{4}\sin(2\alpha_0)\right)\mathbf{u}\mathbf{u}^T\right. \tag{26}$$

$$\left. -\left(\frac{3}{2}\alpha_0 - \frac{1}{4}\sin(2\alpha_0)\right)\mathbf{n}_c(l)\,\mathbf{n}_c(l)^T\right] \tag{27}$$

$$\overleftrightarrow{\bar{w}}_c^{(2)}(l,\mathbf{u}) = \overleftrightarrow{0}, \tag{28}$$

(29)

where $L^* = L/\sigma$, $\alpha_0 = \lim_{b\to 0}\alpha(b) = \arcsin(L/\sigma)$ and $\mathbb{I}$ is the 3×3 identity matrix.

We will restrict ourselves to inhomogeneous fluids in the presence of a one-dimensional external potential $V_{\text{ext}}(z)$, for which the density profile only depends on z and the angle θ between $\hat{z}$ and the direction vector of a particle, where $\hat{z}$ is the direction in which the external potential varies. The integrals in (16) reduce to integrals over z' and θ

$$n_\alpha(z) = \int\int v^{(\alpha)}(z',\theta)\rho(z-z',\theta)\mathrm{d}z'd\theta \tag{30}$$

where the modified weight functions $v^{(\alpha)}$ are obtained analytically by splitting the integrals in (16) into slices perpendicular to the z-axis, over which the weight functions can be integrated as the density only depends on z. The density profile is normalized such that $A\iint\rho(z,\theta)\mathrm{d}zd\theta = N$, where θ runs from 0 to $\pi/2$ due to the up–down symmetry of the dumbbells.

The minimization of the grand potential Ω is performed iteratively, using

$$\rho(z,\theta)\sigma^3 = \exp\left[\mu^* - \beta V_{\text{ext}}(z,\theta) - \beta\frac{\delta\mathcal{F}_{\text{exc}}}{\delta\rho(z,\theta)}\right]. \tag{31}$$

which is equivalent to the minimization criterion $\delta\Omega/\delta\rho = 0$. The functional derivative can be written in terms of convolutions over the weight functions, as described in Ref. 4.

B. Simulations

We use standard Monte Carlo (MC) simulations in the *NVT* ensemble[47] for dumbbells between two walls. In the case of nonzero gravity, we fix the chemical potential μ by performing standard[47] particle insertion and deletion moves in addition to the usual MC moves that modify the positions and orientations of the dumbbells. The system has two hard walls separated by a distance H, such that MC moves that result in $z_{i,\tau} < R = \sigma/2$ or $z_{i,\tau} > H - R$ are rejected for any sphere τ of any dumbbell i, where $z_{i,\tau}$ denotes the z-component of the center of the sphere. We employ periodic boundary conditions in the lateral directions in our simulations. We required around 10^7 MC cycles to obtain enough statistics, preceded by a slightly shorter equilibration, where a cycle consisted of N MC moves. The number of particles in our simulations varied, but was always of the order of a thousand particles, which is sufficient to avoid finite size effects in a fluid phase. Finally, the bulk equation of state of the fluid was measured using *NPT* Monte Carlo simulations[47] without hard walls and with periodic boundary conditions in all three directions.

C. Density and orientational order parameter profiles

From edFMT, the density profile $\rho(z,\theta)$ as a function of z and θ is obtained. In principle, this profile can also be measured in Monte Carlo simulations, but as this is a function of two variables, plotting the results from Monte Carlo and edFMT in the same figure is difficult. Instead, we will make use of the center-of-mass density profile, that is only a function of z,

$$\eta_{\text{com}}(z) \equiv \left\langle \frac{v_{\text{db}}}{A}\sum_i \delta(z-z_i)\right\rangle = \int d\theta\,\sin\theta\;\eta(z,\theta), \tag{32}$$

where the first line denotes the method by which η_{com} is measured in the simulations and the second the way of obtaining it from the $\eta(z,\theta) \equiv v_{\text{db}}\rho(z,\theta)$ obtained from edFMT.

The zz component of the nematic order tensor can also be obtained similarly:

$$Q_{zz}(z) \equiv \left\langle \sum_i\left[\frac{3}{2}\cos^2\theta_i - \frac{1}{2}\right]\delta(z-z_i)\right\rangle \Big/ \left\langle\sum_i\delta(z-z_i)\right\rangle = \int d\theta\,\sin\theta\left(\frac{3}{2}\cos^2\theta - \frac{1}{2}\right)\eta(z,\theta)/\eta_{\text{com}}(z). \tag{33}$$

This parameter $Q_{zz}(z)$ measures the alignment of the particles along the z axis at height z. The orientational order parameter $Q_{zz}(z) = -1/2$ when the orientations of all particles at height z lie in the $x-y$ plane, while $Q_{zz}(z) = 1$ implies perfect alignment with the z-axis for all particles at height z.

IV. RESULTS AND DISCUSSION

A. Fluid equation of state

The edFMT equation of state (EOS) for the homogeneous fluid can be obtained from the free energy (2) for a density profile with $\eta(\mathbf{r},\mathbf{u}) \equiv v_{\rm db}\rho(\mathbf{r},\mathbf{u}) = \eta/4\pi$. For such a constant density profile, the weighted densities can easily be calculated analytically,

$$n_0 = \rho, \tag{34}$$

$$n_1 = \rho R\left(1 + L^* - \frac{1}{2}\arcsin(L^*)\right), \tag{35}$$

$$n_2 = \rho 4\pi R^2(1 + L^*), \tag{36}$$

$$n_3 = \rho\frac{4\pi}{3}R^3\left(1 + \frac{3}{2}L^* - \frac{1}{2}L^{*3}\right)v_{\rm db}, \tag{37}$$

$$\overleftrightarrow{n}_2 = n_2\mathbb{I}/3, \tag{38}$$

while all other weighted densities are zero. Note in particular, that the term proportional to ζ in the free energy (3) is equal to zero, since the $\overleftrightarrow{n}_1$ tensor vanishes. Using these weighted densities, the edFMT equation of state reads

$$z_{\rm FMT} \equiv \frac{\beta P}{\rho} = \frac{1}{1-\eta} + \alpha\frac{\eta}{(1-\eta)^2} + \alpha'\frac{\eta^2}{(1-\eta)^3}, \tag{39}$$

where $\alpha = m_1m_2/m_3$ and $\alpha' = m_2^3/m_3^2$ with $m_\alpha = n_\alpha/\rho$. The form (39) of the FMT equation of state is the same for all particle shapes, where the m_α are the fundamental measures of the particle: m_3 is the volume of the particle, m_2 its surface and, m_1, a characteristic length. The characteristic length m_1 is equal to the mean half width of the particle[50,51] for convex particles. For non-convex particles, the mean half width of a particle is not equal to $m_1 = n_1/\rho = \int K/(4\pi)dA$ in general. For instance for a dumbbell, the mean half width is equal to $R + L/4$, the mean half width of a spherocylinder with the same aspect ratio, instead of n_1/ρ, see Eq. (35). Rosenfeld[49] derived a fundamental measure equation of state from a scaled particle (SP) approach combined with a diagrammatic Percus-Yevick-like theory (PY). This work was performed before Rosenfeld developed the density functional theory version of FMT. Hansen-Goos and Mecke's edFMT is consistent with the SP-PY approach in the sense that for convex particles the same equation of state is obtained. The generalization to non-convex particles can be performed, for the isotropic fluid, either by using the edFMT result from Eq. (35) for the characteristic length, as we have done, or the mean half width, which was Rosenfeld's choice. Furthermore, Rosenfeld also combined his scaled particle theory with the emperical modification to the hard sphere EOS by Carnahan and Starling, resulting in a EOS (SP-CS) that differs from Eq. (39) by an additional term $-(\alpha'/3)\,\eta^3/(1-\eta)^3$.

The equation of state, as measured in Monte Carlo *NPT* simulations is compared to the results from edFMT and Rosenfeld's generalization of Carnahan-Starling (SP-CS), as well as the semi-empirical Tildesley-Streett (TS) EOS (Ref. 48) in Fig. 3. As the TS equation of state is obtained by fitting the exact second virial coefficient and Monte Carlo data, it also fits our simulation results perfectly. The agreement between both the SP-CS and edFMT equations of state and the MC results is good for the smaller aspect ratios, especially at low densities. Being an extension of the Carnahan-Starling equation of state, the SP-CS gives a better fit to the simulation results as the edFMT EOS for high densities and low aspect ratios. For the largest aspect ratio $L^* = 0.9$, the edFMT EOS agrees less well with the MC results, and the agreement with the SP-CS is also not as good as for the lower aspect ratios. For completeness, we note that Nezbeda[52] also obtained an equation of state for dumbbells using a scaled particle approach, but we do not show this EOS in Fig. 3 as it performs worse than the other equations of state.

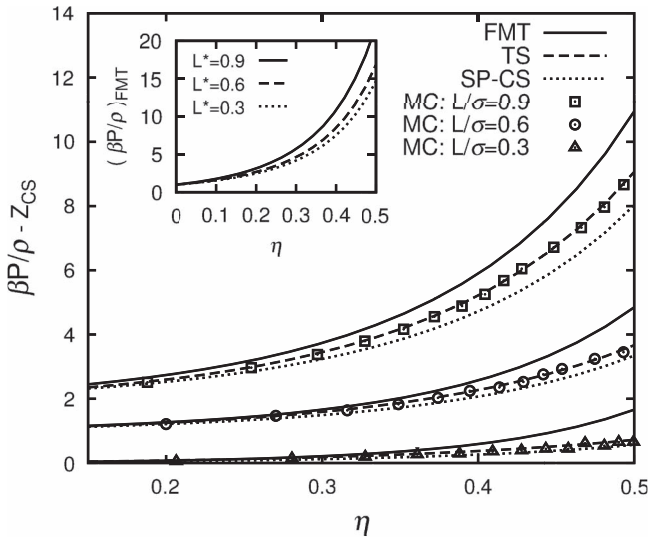

FIG. 3. The fluid equations of state (EOS) of dumbbells with aspect ratios $L/\sigma = 0.3$ (triangles), $L/\sigma = 0.6$ (circles) and $L/\sigma = 0.9$ (squares): the compressibility factor $\beta P/\rho$ versus the packing fraction. We subtracted the Carnahan-Starling equation of state[11] Z_{CS} for hard spheres to clearly show the effect of finite elongation and the results for $L/\sigma = 0.6$ and $L/\sigma = 0.9$ have been shifted upwards for clarity by 1 and 2 respectively. The points are results from *NPT* Monte Carlo simulations, the solid line denotes the edFMT result from this work, the dashed line the semi-empirical Tildesley-Streett EOS (TS) (Ref. 48) and the dotted line, Rosenfeld's scaled particle-Carnahan Starling EOS (SP-CS) (Ref. 49) (see text for a description of the equations of state). The SP-CS EOS is difficult to distinguish from the TS EOS for $L/\sigma = 0.3$. In the inset, we show the unmodified EOS from this work $(\beta P/\rho)_{\rm FMT}$ are shown, again for $L^* = L/\sigma = 0.3$ (dotted line), $L^* = 0.6$ (dashed line) and $L^* = 0.9$ (drawn line).

We have determined that the FMT EOS overestimates the simulation results at low densities primarily because it overestimates the second virial coefficient, which is equal to $\alpha + 1$. We could have added a strictly negative additional term $-(\alpha'/3)\,\eta^3/(1-\eta)^3$ to the edFMT equation of state to obtain a Carnahan-Starling version of FMT. The resulting EOS (not shown) fits the simulation data considerably better than the SP-CS EOS for $\eta \gtrsim 0.3$, especially for $L^* = 0.6$. However, the SP-CS second virial coefficient is much closer to the exact virial coefficient than the edFMT virial coefficient (that is not modified by the additional term). Apparently, the overestimation of the second virial coefficient by edFMT is canceled by the additional $-(\alpha'/3)\,\eta^3/(1-\eta)^3$ term. However, it seems unlikely that the overestimation of the second virial coefficient, which increases with the non-convexity of the particles,

will be canceled by the $-(\alpha'/3)\,\eta^3/(1-\eta)^3$ for other particle shapes than dumbbells. Because we wish to conclude something about general non-convex shapes, we only consider the original edFMT in this work to avoid this (most likely) fortuitous cancellation for dumbbells. However, adjusting edFMT to yield a Carnahan-Starling-like EOS for the isotropic fluid along the lines of Refs. 12 and 53 for anistropic particles and applying it to isotropic and homogeneous fluids of a number of non-convex shapes is certainly an interesting topic for future work.

B. Hard walls

The structure of a fluid confined between two hard walls has been investigated by means of simulations and edFMT. The resulting center-of-mass density profiles are shown in Fig. 4 for three different packing fractions η and three different aspect ratios L/σ. We have used $\zeta = 0$ for the edFMT results. At the lowest packing fraction, the main effect of the elongation of the particles is an entropy reduction when particles are close to the wall due to a decrease in the available orientations. This effect pushes the particles away from the wall, while the presence of the other particles pushes the particles towards the wall. This competition causes the first peak to be located slightly away from $z = \sigma/2$, which is the position of the first peak for hard spheres near a hard wall. As the density increases more peaks in the density profile appear, indicative of layering. For the larger aspect ratios $L/\sigma = 0.6$ and 0.9 and at the highest packing fraction $\eta = 0.5$, the density profile shows an intricate structure as the layering of the spheres of which the dumbbells consist competes with the layering of the center of mass.[43] This causes a splitting of the first peak near the wall, where the two resulting peaks can be ascribed to the primarily horizontal ($z \simeq \sigma/2$) and vertical ($z \simeq [\sigma + L]/2$) orientations. When comparing the profiles for $\eta = 0.5$ and varying L, we note that the layering seems to extend the furthest from the walls for the shortest dumbbells with $L^* = 0.3$. Apparently, the randomness induced by the orientations of the more elongated dumbbells disrupts the layers.

All peaks observed in the profiles obtained from the simulations are reproduced in the FMT results and for all but the highest density, near the wall, the agreement between the two profiles is excellent. Note, that the highest density $\eta = 0.5$ is considerably higher than the densities investigated by Hansen-Goos and Mecke[3,4] for hard spherocylinders, 0.346 at most. Therefore, we cannot be certain that the deviations from the MC results are due to the non-convex nature of the dumbbell, as the theory has not been tested for inhomogeneous systems of convex particles at such high densities.

When we compare our results for the center-of-mass profile with the results obtained by Henderson *et al.*[44] (not shown), we see that both DFTs give a reasonable qualitative agreement for all aspect ratios and densities considered, although it seems that the characteristic splitting of the first peak is absent in the theory of Ref. 44 for the larger aspect ratios. Quantitatively, edFMT also seems to perform a bit better than the older DFT.[44]

C. Nonzero ζ

The edFMT density profiles near a hard wall showed excellent agreement with MC results for spherocylinders with $L/D = 2.5$ and 5, where L is the cylinder length and D the cylinder diameter.[4] The density profiles for the dumbbells from edFMT for $\zeta = 0$ do not show quite as good an agreement with the MC results, see Fig. 5, as in Ref. 4, where the relative deviation was less than 2% for all $z > (L + \sigma)/2$ at $\eta = 0.346$. Our results for higher packing fraction $\eta = 0.5$ have an order of magnitude higher deviation, see Fig. 5. However, the large peak in the relative deviation around $z = 1.2\sigma$ is mainly caused by the small value of the density profile at that position; the absolute value of the deviation at $z \simeq 1.2\sigma$ is not much larger than the deviation at other z positions. As mentioned in Sec. III A 1, the approach for obtaining a nonzero value for ζ proposed by Hansen-Goos and Mecke[4] is to fit the exact excluded volume with the edFMT result. The edFMT excluded volume in the isotropic dumbbell fluid reads

$$v_{\mathrm{edFMT}}(\gamma) = 2v_{\mathrm{db}} + 2m_1 m_2 + \zeta\bar{m}\left(\frac{3}{2}\sin^2\gamma - 1\right), \qquad (40)$$

where m_1 and m_2 were defined in Sec. IV A and γ, the angle between the two dumbbells replaces the indices ν and o in the definition (12). Furthermore, the factor $\bar{m}$ is given by

$$\bar{m} = \frac{\pi}{16}L\sigma^2[2\alpha_0 + \sin(2\alpha_0)](1 - L^{*2})^{3/2}. \qquad (41)$$

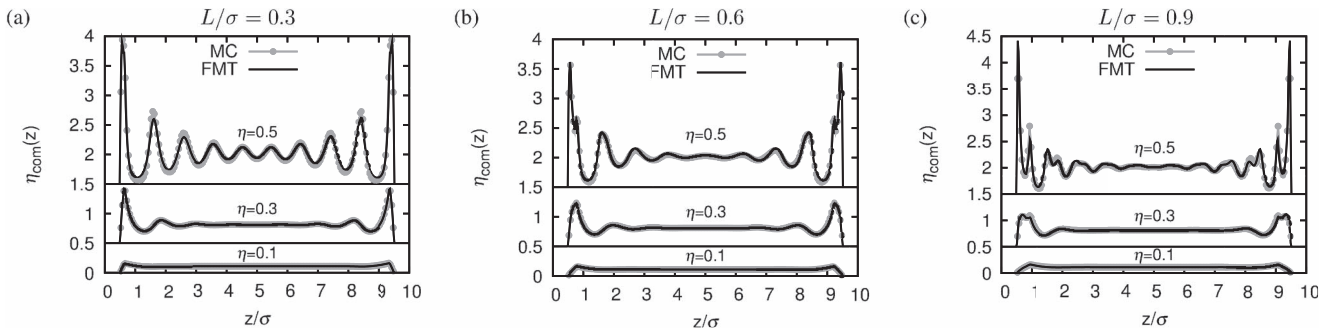

FIG. 4. The center-of-mass density profiles of dumbbells with three different aspect ratios $L^* = 0.3$ (a), $L^* = 0.6$ (b), and $L^* = 0.9$ (c) for three different packing fractions: $\eta = 0.1$, 0.3 and 0.5. The black lines denote the edFMT results, while the circles denote the MC results. The results for $\eta = 0.3$ and 0.5 are shifted upwards by 0.5 and 1.5 respectively for clarity of display.

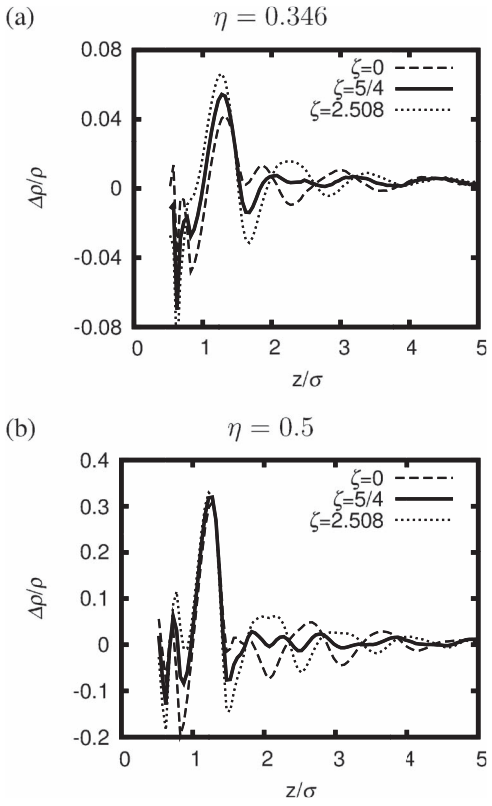

FIG. 5. The difference between the center-of-mass density profiles from edFMT and from simulations divided by the edFMT results for dumbbells between two hard walls and $\zeta = 0$ (dashed line), 5/4 (solid line) and 2.508 (dotted line). Parameters are the same as in Fig. 4(b) except that for (a) $\eta = 0.346$ and for (b) $\eta = 0.5$. Note the difference in scale between (a) and (b).

The exact excluded volume is somewhat involved and is written down in appendix A. One can see from the edFMT excluded volume (40) why fitting the edFMT excluded volume to the exact v_{exc} leads to unphysical values by considering the limit $L \to \sigma$. The exact excluded volume is an increasing function of γ for all nonzero L, while the monotonic increase of Eq. (40) with increasing γ is due to the $(\frac{3}{2}\sin^2\gamma - 1)$ term. The factor $\bar{m}$ goes to zero for $L^* \to 1$, due to the $(1 - L^{*2})^{3/2}$ factor. As a result, the value for $\zeta \sim 1/\bar{m}$ obtained by fitting Eq. (40) to the exact v_{exc} goes to infinity as $L^* \to 1$.

Nevertheless, we can still attempt to minimize the difference between the edFMT and FMT results for the density profile by varying ζ. In Fig. 5, we plot the relative deviation of the edFMT density profile from the results of the MC simulations for $L^* = 0.6$, $\eta = 0.346$ and 0.5 and varying $\zeta = 0$, $\frac{5}{4}$ and 2.508. The latter value for ζ was obtained by minimizing the difference between Eq. (40) and the exact v_{exc}. For any non-convex shape we can define ζ_{CE} as the value for ζ that minimizes the difference between the exact and edFMT excluded volumes for its convex envelope (CE). This value $\zeta_{\text{CE}} = 5/4$ turns out to be the value that gives the smallest deviation for dumbbells, where the convex envelope of a dumbbell is a spherocylinder. However, the result for $\zeta = 1$ (not shown) is nearly indistinguishable from the result for $\zeta = 5/4$. It would be interesting to consider other non-convex shapes to investigate the conjecture that ζ_{CE} is the optimal value for ζ for any non-convex particle.

The largest relative deviation in the density profile around $z = 1.2\sigma$ does not seem to be improved much by changing ζ. Furthermore, considerably less overall improvement could be achieved by choosing a nonzero ζ for $L^* = 0.3$ and 0.9 than for $L^* = 0.6$, although $\zeta = 5/4$ at least did not deteriorate the results significantly. The $\overleftrightarrow{n}_1$ tensor does not have to be calculated if ζ is zero. Considering the limited improvement achieved by a non-zero ζ, we do not think that choosing a non-zero ζ is worth the extra effort of calculating $\overleftrightarrow{n}_1$ for inhomogeneous fluids of dumbbells. Therefore, we use $\zeta = 0$ in the remainder of this paper.

D. Confinement

The effect of the wall spacing H has been studied in edFMT by systematically varying H/σ between 1.025 and 4.975 with steps of 0.05. Furthermore, the edFMT results are compared to the MC results for a few of the smaller spacings, H/σ=1.6, 2 and 2.6, where the effects of the confinement are the largest and, therefore, the theory and the simulations are expected to differ the most. The agreement between results from MC and edFMT is surprisingly good, as shown in Fig. 6(a), which agrees with the observations in the previous section for this aspect ratio $L^* = 0.6$ and packing fraction η

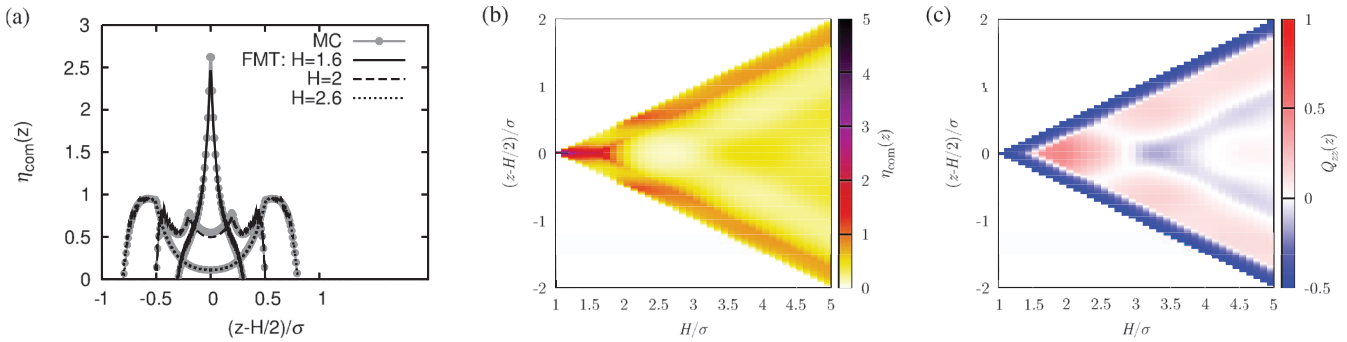

FIG. 6. (a) The center-of-mass density profiles for dumbbells with $L^* = 0.6$ in thin slits with $H/\sigma = 1.6$ (solid), 2 (dashed) and 2.6 (dotted) as a function of $z - H/2$, such that the center of the slit always lies at zero. The black lines denote the edFMT results, while the circles denote the MC results. (b) A color plot of the density from edFMT as a function of $z - H/2$ and the wall separation H, such that each vertical slice corresponds to a density profile for a different value of H. (c) A color plot of the orientational order parameter from edFMT, where $Q_{zz}(z) = 1$ (red) denotes perfect alignment with the z axis and $Q_{zz}(z) = -1/2$ (blue) for dumbbells with orientations in the $x - y$ plane. The average orientation at $z = H/2$ oscillates between horizontal and vertical, starting from horizontal at $H \sim \sigma$. For all three plots, the packing fraction $\eta = 0.3$ was used and the parameter ζ was set to zero.

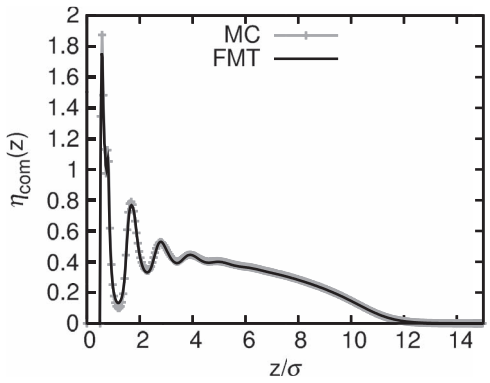

FIG. 7. The center-of-mass density profile, in units of the volume of a dumbbell, as a function of the height z for dumbbells under gravity with $L^* = 0.6$, $\mu^* = 20$ and $g^* = 2$. Simulation results are denoted by the gray crosses and the edFMT results (with $\zeta = 0$) by the black line.

$= 0.3$. The good agreement allows us to study the dependence of the structure on H in greater detail using only the theory in Fig. 6(b). It can be seen that the positions of the peaks in the density profile are complicated functions of the height H.

For $H \sim \sigma$, a single peak appears trivially and the particles have to be parallel to the wall. As H increases, the peak broadens at first, as the particles start to sample more orientations, see Fig. 6(c). However, the peak narrows again when $H \sim \sigma + L$. Simultaneously, the particles align with the z-axis. For yet larger H, the middle peak splits, and seems to be periodically appearing, splitting and disappearing as a function of H. The orientations of the particles also seem to oscillate between the vertical and the horizontal. The periods of the oscillations in both the density and the orientational order are both about σ, which indicates that the oscillatory behavior is related to the spheres that constitute the dumbbells.

E. Gravity

In Fig. 7, we compare results from grand canonical Monte Carlo simulations with edFMT for dumbbells under gravity. To our knowledge, this is the first time density functional theory is applied to this system. We show only the results for $g^* = 2$, $\mu^* = 20$, and $L^* = 0.6$, as the density profiles for different gravitational force, chemical potential and L are similar, except for the behavior at the wall. Furthermore, the behavior at the wall is similar to the results obtained in the absence of gravity in the sections above, compare Fig. 4(b) for $\eta = 0.5$ with Fig. 7. The bulk density corresponding to $\mu^* = 20$ is $\eta = 0.491$ for FMT and the MC bulk packing fraction, which differs from the FMT packing fraction due to the differences between the bulk equations of state, is 0.500. The difference of about 0.01 between the volume fractions causes a small additional error in the edFMT density profile under gravity compared to the results with two hard walls, where the average packing fraction was used as input parameter. However, this effect seems to be small, which can be seen by comparing the deviation between the MC data and the theory in the absence of gravity, shown in Fig. 4(b) for $\eta = 0.5$, with that for dumbbells under gravity in Fig. 7.

V. CONCLUSIONS

We have applied the edFMT density functional theory, recently developed for anisotropic hard particles by Hansen-Goos and Mecke,[3,4] to inhomogeneous fluids of hard dumbbells in a slit and under gravity. The edFMT theory features a free parameter ζ, which has to be nonzero for very elongated particles to allow for a stable nematic phase. Adjusting the free parameter ζ in edFMT by fitting the edFMT excluded volume to the exact excluded volume has been shown to lead to values for ζ that are unrealistically large, presumably because the full theory is not valid for non-convex particles, such as dumbbells. Fortunately, the theory with $\zeta = 0$ gives excellent results when comparing with Monte Carlo simulations for packing fractions similar to those studied before.[4] The agreement is somewhat worse than that obtained for spherocylinders in Ref. 4, but it is better than the results obtained for dumbbells in a slit with a previous density functional theory study of hard dumbbells near a hard wall.[44] At very large packing fraction, $\eta = 0.5$, the theory still predicts the positions of the various peaks well, but does not always predict the correct height for the peaks. We investigated the possibility of choosing a nonzero value for ζ, and obtained some improvement compared to $\zeta = 0$. However, a nonzero value for ζ leads to additional effort in evaluating the free energy functional, which does not seem justified considering the limited effect for inhomogeneous fluids of particles which are not very elongated, like dumbbells. For particles with more extreme aspect ratios, we propose to set ζ equal to the value of ζ which is optimal for the convex envelope of the particle. Also, a nonzero ζ might be required to accurately model crystals of anisotropic particles, which is beyond the scope of this work. Finally, the density profile was shown to depend on the separation between the two walls (in the absence of gravity) in a non-trivial manner. Surprisingly, two walls with a separation just above $L + \sigma$ induce the dumbbells to align perpendicular to the walls, while a single hard wall always causes alignment parallel with the wall for any rod-like particle.

The FMT-density functional for hard dumbbells, which was constructed and explored in this paper, can serve as a starting point for further studies. These future topics should include the full bulk freezing diagram including plastic and full crystalline phases of hard dumbbells. The functional itself might be improved by adjusting it such that it yields the excellent Carnahan-Starling equation for the homogeneous fluid in the hard-sphere limit.[12,53] For an additional attractive interaction which possibly lead to gas-liquid phase separation, our functional can be used as a reference system the attractions being treatable within a mean-field perturbation theory.[54–56] Furthermore, a dipolar interaction force[57] can be added on top of the dumbbell and can again be treated in DFT by a mean-field theory.[58] Moreover, Brownian dynamics (both translational and orientational)[59] can be explored by dynamical density functional theory where a good static functional is needed as an input.[20,21,60] Finally other particle shapes, such as platelets,[61] cubes,[62] tetrahedra,[63] or helical particles[64] can

be described using FMT-like functionals. This finally leads to a full microscopic theory of the phase behavior of anisometric particles.

Finally, it is important to note that a general theory which connects the shape of particles to their phase behavior is important to predict new meso-structures with novel optical, rheological and electric and magnetic properties. For example, open diamond crystals are ideal candidates for photonic crystals[65] and one might tailor optical band-gap materials by selecting colloidal particles with a certain shape[66,67] which favor open crystalline phases. Conversely, one could force existing anisotropic particles to crystallize into high-symmetry crystal structures such as BCC and FCC using external fields, which may lead to a high-quality photonic crystal for specific anisotropic particles. The excellent calculated photonic properties for oriented dumbbells on FCC (Refs. 68 and 69) and BCC (Ref. 69) lattices are quite promising in that respect.

ACKNOWLEDGMENTS

The SFB-TR6 program (project D3) is gratefully acknowledged for financial support.

APPENDIX A: THE EXCLUDED VOLUME OF HARD DUMBBELLS

The second virial coefficient, one half times the integral of the excluded volume over the angle between the dumbbells, has been calculated by Isihara.[70] The only modification in our calculation of the excluded volume is to not integrate over this angle. This leads to a rather complicated looking excluded volume,

$$v_{\text{exc}}^{\text{exact}} = v_{\text{lens}}(2z_0, 2\sigma) - 2v_{\text{lens}}(L, 2\sigma) + 2z_0L^2\sin\gamma + 4\pi\sigma^3 - 4I(r_0, L) - 2I(r_0, 2L\sin(\gamma/2)), \tag{A1}$$

where $r_0 = L/[2\cos(\gamma/2)]$, $z_0 = \sqrt{\sigma^2 - r_0^2}$ and v_{lens} denotes the volume of the lens shaped intersection between two spheres of diameter σ at a distance d,

$$v_{\text{lens}}(d, \sigma) = \frac{\pi}{12}(2\sigma^3 - 3d\sigma^2 + d^3). \tag{A2}$$

Furthermore, $I(r, d)$ denotes an integral, which can be calculated analytically using the results of Ref. 70. After some simplification, the result is

$$I(r, d) = \frac{d}{3}\sqrt{\sigma^2 - r^2}\sqrt{4r^2 - d^2} + \frac{4}{3}\sigma^3 \arctan\left(\frac{\sigma\xi}{d}\right) - 2\arccos\left(\frac{d}{2r}\right)\frac{2\sigma^2 + r^2}{3}\sqrt{\sigma^2 - r^2} - d(\sigma^2 - d^2/12)\arctan\left(\frac{\xi}{2}\right), \tag{A3}$$

where $\xi = \sqrt{4r^2 - d^2}/\sqrt{\sigma^2 - r^2}$.

APPENDIX B: ZERO DIMENSIONAL CAVITIES

The fundamental measure theory for hard spheres by Tarazona[10] was derived from the condition that the theory gives the correct result for the inhomogeneous densities that result in confining particles in a collection of zero-dimensional cavities, each of which is just large enough to hold a single particle. We will extend his derivation to anisotropic hard particles. To be exact, we will consider the external potential

$$V_\nu^{\text{ext}}(\mathbf{r}) = \lim_{\delta\to 0}\sum_k \delta_{\nu,\nu(k)} \times \begin{cases} 0 & |\mathbf{r} - \mathbf{r}_k| \le \delta \\ \infty & \text{otherwise} \end{cases}, \tag{B1}$$

where a particle is tightly enclosed by cavity k if its position is $\mathbf{r}_k$ and its combined species and orientation is $\nu(k)$ and $\delta_{\nu,o}$ is a generalization of the Kronecker delta, such that $\sum_\nu f_\nu \delta_{\nu,o} = f_o$ with $\sum_\nu$ a combination of a sum over the species and integrals over the orientations as discussed in Sec. III A. The resulting inhomogeneous density profile consists of a sum of delta functions

$$\rho_\nu(\mathbf{r}) = \sum_k N_k \delta(\mathbf{r} - \mathbf{r}_k)\delta_{\nu,\nu(k)}. \tag{B2}$$

In the case of overlapping cavities, $N \equiv \sum_k N_k \le 1$ and the exact excess free energy is known to be[9]

$$\varphi_0(N) = N + (1 - N)\log(1 - N). \tag{B3}$$

To completely determine the functional we will need to consider three overlapping cavities, but in the spirit of Ref. 10, we will start with one cavity and add cavities one-by-one.

1. A single cavity

For a single cavity, the generalization of the free energy functional of hard spheres[9] is

$$\mathcal{F}_1 = -\int \mathrm{d}\mathbf{r}\log[1 - n_3(\mathbf{r})] \times \sum_\nu \int \mathrm{d}\mathbf{r}_0 w_2(\mathbf{r}_0)\rho_\nu(\mathbf{r} - \mathbf{r}_0)\frac{K_\nu(\hat{r}_0)}{4\pi}. \tag{B4}$$

The integral over $\mathbf{r}$ can be performed analytically, resulting in

$$\mathcal{F}_1 = \varphi_0(N)\int_{\partial\mathcal{B}_1} \mathrm{d}A\frac{K_1}{4\pi}, \tag{B5}$$

where $\mathcal{B}_i$ is the body with the orientation, position and species such that it just fits inside cavity i and $\partial\mathcal{B}_i$ is its surface. This can be shown to be equal to $\varphi_0(N)$ for convex particles with the use of the Gauss-Bonnet theorem, which we will write in a slightly more general form here (cf. Eq. (13)),

$$\int_S K\,\mathrm{d}A + \sum_k \int_{\partial S_k} \kappa_g \mathrm{d}s + \sum_n \angle_n = 2\pi\chi(S), \tag{B6}$$

where S is a surface of any body bounded by an oriented curve ∂S consisting of M smooth sections ∂S_k, while the curve turns by $\angle_n$ at the intersection between sections ∂S_{n-1} and ∂S_n (and $\partial S_0 \equiv \partial S_M$). Furthermore, K is the Gaussian curvature and κ_g is the geodesic curvature on the smooth sections of

∂S. If we take for S the surface $\partial\mathcal{B}_1$, the free energy $\mathcal{F}_1$ reduces to $\varphi_0(N)\chi(\partial\mathcal{B}_1)/2$ ($\partial\mathcal{B}_1$ has no boundary). All convex shapes and many non-convex shapes $\mathcal{B}$ satisfy $\chi(\partial\mathcal{B}) = 2$, notable exceptions being tori and other handle bodies that have $\chi(\partial\mathcal{B}) = 2(1-n)$, with n the number of handles. With these exceptions, $\mathcal{F}_1$ reduces to the correct free energy for a single zero-dimensional cavity. Furthermore, $\mathcal{F}_1$ can be written in terms of the weighted densities n_0 and n_3,[4] which allows it to be evaluated efficiently for any density profile $\rho_\nu(\mathbf{r})$. In the remainder of this section, we will restrict the discussion to shapes topologically equivalent to a sphere, that is, those shapes that have $\chi(\partial\mathcal{B}_1) = 2$.

2. Two cavities

For two cavities, $\mathcal{F}_1$ does not give the correct zero dimensional free energy $\varphi_0(N)$ if $\mathcal{B}_1$ overlaps with $\mathcal{B}_2$. In fact, the free energy $\mathcal{F}_1$ becomes

$$\mathcal{F}_1 = \varphi_0(N) + \phi_1(N_1, N_2)\left[\sum_{i\neq j}\int_{\partial\mathcal{B}_i\cap\mathcal{B}_j}\frac{K_j}{4\pi}\mathrm{d}A - 1\right], \quad \text{(B7)}$$

where we have defined $\phi_1(N_1, N_2) \equiv \phi_0(N_1 + N_2) - \phi_0(N_1) - \phi_0(N_2)$. The Gauss-Bonnet theorem can be applied to rewrite the difference between $\mathcal{F}_1$ and the exact free energy $\varphi_0(N)$, where we use for S the surface $\partial\mathcal{B}_i \cap \mathcal{B}_j$, *i.e.* the part of the surface of i that is inside j. The boundary of this surface, $\partial\mathcal{B}_i \cap \partial\mathcal{B}_j$, is smooth (*i.e.* $M = 1$). Applying the Gauss-Bonnet theorem in this way, the difference between the exact free energy $\varphi_0(N)$ and $\mathcal{F}_1$ becomes

$$\varphi_0(N) - \mathcal{F}_1 = \phi_1(N_1, N_2)\left[\int_{\partial\mathcal{B}_1\cap\partial\mathcal{B}_2}\frac{\kappa_1^g + \kappa_2^g}{4\pi}\mathrm{d}l + 1 - \frac{1}{2}\sum_{i\neq j}\chi\left(\partial\mathcal{B}_i\cap\mathcal{B}_j\right)\right]. \quad \text{(B8)}$$

For convex particles, it has been shown that

$$\sum_{i\neq j}\chi(\partial\mathcal{B}_i\cap\mathcal{B}_j) = \chi\left(\partial[\mathcal{B}_1\cap\mathcal{B}_2]\right) + \chi(\partial\mathcal{B}_1\cap\partial\mathcal{B}_2) = 2$$

in Sec. III A 2. Therefore, the last two terms in the square brackets cancel for convex particles in Eq. (B8). Using the explicit expression for the geodesic curvature from Ref. 4, the remaining term can be written as

$$\varphi_0(N) - \mathcal{F}_1 = \int \mathrm{d}\mathbf{r}[1 - n_3(\mathbf{r})]^{-1}\sum_{\nu_1,\nu_2}\int\int \mathrm{d}\mathbf{r}_1\mathrm{d}\mathbf{r}_2 \times\left[\prod_{k=1}^{2} w_2(\mathbf{r}_k)\rho_{\nu_k}(\mathbf{r}-\mathbf{r}_k)\right]\mathcal{K}^{(1)}_{\nu_1,\nu_2}(\hat{r}_1,\hat{r}_2), \quad \text{(B9)}$$

where the "kernel" $\mathcal{K}^{(1)}_{\nu,o}$ is given by

$$\mathcal{K}^{(1)}_{\nu,o} = \frac{H_\nu}{4\pi}[1 - \mathbf{n}_\nu\cdot\mathbf{n}_o] - \frac{\Delta\kappa_\nu}{4\pi}\frac{(\mathbf{v}_\nu^I\cdot\mathbf{n}_o)^2 - (\mathbf{v}_\nu^{II}\cdot\mathbf{n}_o)}{1 - \mathbf{n}_\nu\cdot\mathbf{n}_o}, \quad \text{(B10)}$$

and it is to be understood that the quantities with subscript $\tau = \nu, o$ depend on the direction $\hat{r}_\tau$. The kernel $\mathcal{K}^{(1)}_{\nu,o}$ can be simplified by approximating $1/(1 - \mathbf{n}_\nu\cdot\mathbf{n}_o) \simeq \zeta$ with ζ an adjustable constant. After this approximate simplification, the free energy difference $\varphi_0(N) - \mathcal{F}_1$ can be written in terms of weighted densities.[4] Now, we can trivially correct the free energy functional $\mathcal{F}_1$ by adding a second term $\mathcal{F}_2 \equiv \varphi_0(N) - \mathcal{F}_1$ which can be evaluated with similar ease as the first term $\mathcal{F}_1$ for a general density profile $\rho_\nu(\mathbf{r})$. For a single cavity, $\mathcal{F}_2$ is zero (also after the approximation), as all normals are equal and $\mathbf{v}_1^I$ and $\mathbf{v}_1^{II}$ are perpendicular to $\mathbf{n}_1$.

3. Three cavities

The calculation for three delta functions is a bit involved. The free energy becomes

$$\mathcal{F}_1 + \mathcal{F}_2 = \varphi_0(N) + \sum_{\{ij\}}\phi_1(N_i, N_j)\left[\frac{\chi(\delta[\mathcal{B}_i\cap\mathcal{B}_j])}{2} - 1\right] + \phi_2(N_1, N_2, N_3)\sum_{\{ijk\}}\left[\int_{\partial\mathcal{B}_i\cap\mathcal{B}_j\cap\mathcal{B}_k}\frac{K_i}{4\pi}\mathrm{d}A + \int_{\partial\mathcal{B}_i\cap\partial\mathcal{B}_j\cap\mathcal{B}_k}\frac{\kappa_i^g + \kappa_j^g}{4\pi}\mathrm{d}l - 1\right], \quad \text{(B11)}$$

where $\{ij\}$ denotes all pairs (1, 2), (2, 3), and (3, 1), while $\{jkl\}$ denotes all triplets (1, 2, 3), (2, 3, 1), and (3, 1, 2). Additionally, we defined $\phi_2(N_1, N_2, N_3) = \varphi_0(\sum_i N_i) - \sum_{\{ij\}}\varphi_0(N_i + N_j) + \sum_i\varphi_0(N_i)$. Expression (B11) is obtained by applying the Gauss-Bonnet theorem (B6) in a similar way as above with $S = \partial\mathcal{B}_i \cap \mathcal{B}_j$ and subsequently using the equality $\mathcal{K}_{\nu,o} + \mathcal{K}_{o,\nu} = \kappa_\nu^g + \kappa_o^g$, which holds on the intersection between the surfaces of ν and o. The last term in Eq. (B11) can also be simplified using the Gauss-Bonnet theorem (B6) with $S = \partial\mathcal{B}_i \cap \mathcal{B}_j \cap \mathcal{B}_k$,

$$\int_{\partial\mathcal{B}_i\cap\mathcal{B}_j\cap\mathcal{B}_k}\frac{K_i}{4\pi}\mathrm{d}A + \int_{\partial\mathcal{B}_i\cap\partial\mathcal{B}_j\cap\mathcal{B}_k}\frac{\kappa_i^g + \kappa_j^g}{4\pi}\mathrm{d}l = \frac{1}{2}\chi(\partial\mathcal{B}_i\cap\mathcal{B}_j\cap\mathcal{B}_k) - \sum_n\frac{\angle_n}{4\pi}. \quad \text{(B12)}$$

where $\angle_n$ is the angle by which the curve $\partial[\partial\mathcal{B}_i \cap \mathcal{B}_j \cap \mathcal{B}_k]$ turns at the nth point in the intersection $\partial\mathcal{B}_i \cap \partial\mathcal{B}_j \cap \partial\mathcal{B}_k$, see Fig. 8. It remains to combine the $\chi(\partial\mathcal{B}_i \cap \mathcal{B}_j \cap \mathcal{B}_k)$, which, for each triplet, is the Euler index of a bounded surface possibly consisting of multiple disconnected regions, into the Euler index of a single surface. The intersection between any number of convex bodies is also a convex body, so the surface $\partial[\mathcal{B}_1 \cap \mathcal{B}_2 \cap \mathcal{B}_3] = \bigcup_{\{ijk\}}\partial\mathcal{B}_i \cap \mathcal{B}_j \cap \mathcal{B}_k$, will have Euler characteristic 2 for convex $\mathcal{B}_i$. Its Euler characteristic can be written as

$$\chi\left(\partial[\mathcal{B}_i \cap \mathcal{B}_j \cap \mathcal{B}_k]\right) = \sum_{\{ijk\}}\chi(\partial\mathcal{B}_i\cap\mathcal{B}_j\cap\mathcal{B}_k) - \sum_{\{ijk\}}\chi(\partial\mathcal{B}_i\cap\partial\mathcal{B}_j\cap\mathcal{B}_k) + \chi(\partial\mathcal{B}_i\cap\partial\mathcal{B}_j\cap\partial\mathcal{B}_k), \quad \text{(B13)}$$

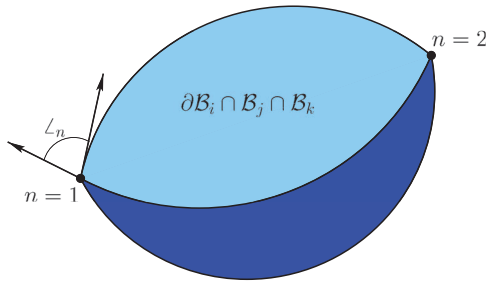

FIG. 8. The intersection between the convex bodies $\mathcal{B}_i$, $\mathcal{B}_j$ and $\mathcal{B}_k$ in the simplest case, where the surface of the intersection consists of three parts, two of which are denoted by the lighter and darker regions in this figure, while the last part is obscured by the other two. The lines of intersection between two parts of the surface, e.g., $\partial\mathcal{B}_i \cap \partial\mathcal{B}_j \cap \mathcal{B}_k$ are indicated by the black lines, while the dots denote the intersection points $\partial\mathcal{B}_i \cap \partial\mathcal{B}_j \cap \partial\mathcal{B}_k$. The angle $\angle_n$ by which the curve $\partial[\partial\mathcal{B}_i \cap \mathcal{B}_j \cap \mathcal{B}_k]$ turns is indicated for $n = 1$.

which is similar to the Euler characteristic of a polyhedron: $\chi = F - E + V$, where F is the number of faces, E is the number of edges and V is the number of vertices. Unlike polyhedra, our surface $\partial[\mathcal{B}_i \cap \mathcal{B}_j \cap \mathcal{B}_k]$ has curved edges and faces in general, which allows for the possibility of closed loop-like edges, which have a vanishing contribution to the sum over the edges as they have Euler characteristic zero. Furthermore, a vertex is always connected by three edges, which makes it possible to relate the number of edges E' not forming a loop to the number of vertices V for $\partial[\mathcal{B}_i \cap \mathcal{B}_j \cap \mathcal{B}_k]$. In fact, each edge connects two vertices, which it shares with two other edges, so $E' = \frac{3}{2}V$. So finally,

$$\sum_{\{ijk\}} \chi(\partial\mathcal{B}_i \cap \mathcal{B}_j \cap \mathcal{B}_k) = \chi\left(\partial[\mathcal{B}_1 \cap \mathcal{B}_2 \cap \mathcal{B}_3]\right) + \frac{V}{2}. \tag{B14}$$

Inserting this expression and Eq. (B12) in the expression (B11) for $\mathcal{F}_1 + \mathcal{F}_2$ and rearranging the sums over pairs $\{jkl\}$ to run over vertices v instead, we obtain

$$\begin{aligned}\mathcal{F}_1 + \mathcal{F}_2 = \varphi_0(N) &+ \sum_{\{ij\}} \phi_1(N_i, N_j)\left[\frac{\chi(\delta[\mathcal{B}_i \cap \mathcal{B}_j])}{2} - 1\right] \\ &+ \phi_2(N_1, N_2, N_3)\left[\frac{\chi\left(\partial[\mathcal{B}_1 \cap \mathcal{B}_2 \cap \mathcal{B}_3]\right)}{2} - 1\right. \\ &\left. - \frac{1}{4\pi}\sum_{v=1}^{V}\left(2\pi - \sum_{m=1}^{3}\angle_v^m\right)\right],\end{aligned} \tag{B15}$$

where v is a vertex and m runs over the three surfaces intersecting at v. The angle $\angle_v^m$ can be expressed in terms of the normals $\mathbf{n}_v^{(m)}$ on surface m and the ones on the other two surfaces $\mathbf{n}_v^I$ and $\mathbf{n}_v^{II}$, by

$$\angle_v^m = \arccos\left[(\mathbf{n}_v^I \widehat{\times} \mathbf{n}_v^{(m)}) \cdot (\mathbf{n}_v^{(m)} \widehat{\times} \mathbf{n}_v^{II})\right]. \tag{B16}$$

This angle is the angle of the corner of surface m at v and is equal to π minus the angle that the path along the boundary of surface m makes in v. The interpretation of $2\pi - \sum_{m=1}^{3}\angle_v^m$ is the amount by which the three angles fail to add up to 2π (which would be zero if surfaces m, I and II were co-planar).

Analogous to the two-shell problem, the free energy can be corrected by adding a third term to the free energy involving three weight functions,

$$\begin{aligned}\mathcal{F}_3 = &\int \mathrm{d}\mathbf{r}[1 - n_3(\mathbf{r})]^{-1} \sum_{\nu_1,\nu_2,\nu_3} \iiint \mathrm{d}\mathbf{r}_1\mathrm{d}\mathbf{r}_2\mathrm{d}\mathbf{r}_3 \\ &\times \left[\prod_{k=1}^{3} w_2(\mathbf{r}_k)\rho_{\nu_k}(\mathbf{r} - \mathbf{r}_k)\right] \mathcal{K}^{(2)}_{\nu_1,\nu_2,\nu_3}(\hat{r}_1, \hat{r}_2, \hat{r}_2),\end{aligned} \tag{B17}$$

where the function $\mathcal{K}^{(2)}_{\nu_1,\nu_2,\nu_3}$ is given by

$$\begin{aligned}\mathcal{K}^{(2)}_{\nu_1,\nu_2,\nu_3} = &\frac{|\mathbf{n}_{\nu_1} \cdot (\mathbf{n}_{\nu_2} \times \mathbf{n}_{\nu_3})|}{24\pi} \\ &\times\left[2\pi - \sum_{\{ijk\}} \arccos\left[(\mathbf{n}_{\nu_i} \widehat{\times} \mathbf{n}_{\nu_j}) \cdot (\mathbf{n}_{\nu_j} \widehat{\times} \mathbf{n}_{\nu_k})\right]\right].\end{aligned} \tag{B18}$$

The sum of the three free energy terms $\mathcal{F}_1 + \mathcal{F}_2 + \mathcal{F}_3$ is approximately equal to the correct free energy $\varphi_0(N)$ for convex particles which have $\chi(\partial[\mathcal{B}_i \cap \mathcal{B}_j]) = \chi(\partial[\mathcal{B}_i \cap \mathcal{B}_j \cap \mathcal{B}_k]) = 2$. Note, that the kernel $\mathcal{K}^{(2)}$ vanishes when any two of $\mathbf{n}_\nu$, $\mathbf{n}_o$ or $\mathbf{n}_\varpi$ are equal and, therefore, the free energy $\mathcal{F}_3$ vanishes in the cases of one and two delta peaks. As $\mathcal{F}_1 + \mathcal{F}_2$ already give the approximately correct result for one and two delta peaks, this means that the sum $\mathcal{F}_1 + \mathcal{F}_2 + \mathcal{F}_3$ also gives the correct result in this case.

The kernel $\mathcal{K}^{(2)}$ can not be written in terms weighted densities, because of the arccos and the $|\cdot|$. Therefore, we expand $\mathcal{K}^{(2)}$ in powers of $\mathbf{n}_i \cdot \mathbf{n}_j$ up to terms of order $(\mathbf{n}_i \cdot \mathbf{n}_j)^3$. However, we must make sure that we do not lose the property that $\mathcal{F}_3 = 0$ for one or two delta peaks. This means we have to neglect some of the terms in the expansion which do not vanish in this case. The final result for the approximated kernel is

$$\mathcal{K}^{(2)}_{\nu_1,\nu_2,\nu_3} = \zeta_1' \prod_{\{ij\}}\left(1 - \mathbf{n}_{\nu_i} \cdot \mathbf{n}_{\nu_j}\right) + \zeta_2'\left[\mathbf{n}_{\nu_1} \cdot \left(\mathbf{n}_{\nu_2} \times \mathbf{n}_{\nu_3}\right)\right]^2, \tag{B19}$$

where the constants $\zeta_1' = (24\pi)^{-1}$ and $\zeta_2' = (\pi/2 - 1)\zeta_1'$ are introduced. For hard spheres, a similar expression, but with different constants ζ_k', was derived by demanding that the direct correlation function and the equation of state of the isotropic and homogeneous fluid were equal to the Percus-Yevick results. Note, that we did not have to consider the direct correlation function of the fluid here, but rather derived the form of the functional completely from the zero-dimensional limit. However, as noted by Roth,[71] the zero-dimensional limit can lead to a functional which does not give very good results for the fluid. In this case, we have to renormalize both terms in the kernel $\mathcal{K}^{(2)}$ to obtain the Percus-Yevick equation of state and the corresponding direct correlation function of the fluid in the hard sphere limit. The corresponding values for ζ_k' are $\zeta_1' = 1/(16\pi)$ and $\zeta_2' = -\zeta_1'$. With these values for ζ_k', the functional $\mathcal{F}_1 + \mathcal{F}_2 + \mathcal{F}_3$ reduces to the edFMT functional (2) of Hansen-Goos and Mecke.[3] The resulting equation of state of the fluid is equal to the

fundamental measure version of the scaled particle equation of state,[49] which shows good agreement with the results from simulations. It remains to be seen if the direct correlation function corresponding to the kernel obtained from the hard sphere limit also reduces to the fundamental-measure scaled-particle result.[49]

In this appendix, we have shown that the edFMT functional gives an approximately correct free energy for collections of cavities containing *convex* particles. For non-convex particles, the additional approximations $\chi(\partial[\mathcal{B}_i \cap \mathcal{B}_j]) \simeq 2$ and $\chi(\partial[\mathcal{B}_i \cap \mathcal{B}_j \cap \mathcal{B}_k]) \simeq 2$ have to be made, which are not bad approximations as long as there are relatively few configurations for which the Euler characteristics differ from 2.

[1] R. Evans, Adv. Phys. **28**, 143 (1979).
[2] P. Tarazona, J. Cuesta, and Y. Martínez-Ratón, in *Theory and Simulation of Hard-Sphere Fluids and Related Systems*, edited by A. Mulero (Springer, Berlin/Heidelberg, 2008).
[3] H. Hansen-Goos and K. Mecke, Phys. Rev. Lett. **102**, 018302 (2009).
[4] H. Hansen-Goos and K. Mecke, J. Phys. Condens.: Matter. **22**, 364107 (2010).
[5] H. Löwen, Physics Reports **237**, 249 (1994).
[6] P. Tarazona, Phys. Rev. Lett. **84**, 694 (2000).
[7] Y. Singh, Physics Reports **207**, 351 (1991).
[8] Y. Rosenfeld, Phys. Rev. Lett. **63**, 980 (1989).
[9] Y. Rosenfeld, M. Schmidt, H. Löwen, and P. Tarazona, Phys. Rev. E **55**, 4245 (1997).
[10] P. Tarazona and Y. Rosenfeld, Phys. Rev. E **55**, R4873 (1997).
[11] N. F. Carnahan and K. E. Starling, J. Chem. Phys. **51**, 635 (1969).
[12] R. Roth, R. Evans, A. Lang, and G. Kahl, J. Phys. Condens.: Matter. **14**, 12063 (2002).
[13] M. Oettel, S. Görig, A. Härtel, H. Löwen, M. Radu, and T. Schilling, Phys. Rev. E **82**, 051404 (2010).
[14] A. Poniewierski and R. Hołyst, Phys. Rev. Lett. **61**, 2461 (1988).
[15] H. Graf and H. Löwen, J. Phys. Condens.: Matter. **11**, 1435 (1999).
[16] P. Bolhuis and D. Frenkel, J. Chem. Phys. **106**, 666 (1997).
[17] M. Schmidt, Phys. Rev. E **63**, 050201 (2001).
[18] A. Esztermann, H. Reich, and M. Schmidt, Phys. Rev. E **73**, 011409 (2006).
[19] Y. Rosenfeld, Phys. Rev. E **50**, R3318 (1994).
[20] A. Härtel and H. Löwen, J. Phys. Condens. Matter. **22**, 104112 (2010).
[21] A. Härtel, R. Blaak, and H. Löwen, Phys. Rev. E **81**, 051703 (2010).
[22] M. Schmidt, Phys. Rev. E **60**, R6291 (1999).
[23] B. Groh and M. Schmidt, J. Chem. Phys. **114**, 5450 (2001).
[24] S. Glotzer and M. Solomon, Nat. Mater. **6**, 557 (2007).
[25] P. M. Johnson, C. M. van Kats, and A. van Blaaderen, Langmuir **21**, 11510 (2005).
[26] E. B. Mock, H. De Bruyn, B. S. Hawkett, R. G. Gilbert, and C. F. Zukoski, Langmuir **22**, 4037 (2006).
[27] S. H. Lee, S. J. Gerbodea, B. S. John, A. K. Wolfgang, F. A. Escobedo, I. Cohen, and C. M. Liddell, J. Mater. Chem. **18**, 4912 (2008).
[28] E. B. Mock and C. F. Zukoski, Langmuir **23**, 8760 (2007).
[29] S. J. Gerbode, S. H. Lee, C. M. Liddell, and I. Cohen, Phys. Rev. Lett. **101**, 058302 (2008).
[30] S. J. Gerbode, U. Agarwal, D. C. Ong, C. M. Liddell, F. Escobedo, and I. Cohen, Phys. Rev. Lett. **105**, 078301 (2010).
[31] A. F. Demirörs, P. M. Johnson, C. M. van Kats, A. van Blaaderen, and A. Imhof, Langmuir **26**, 14466 (2010).
[32] C. Vega, E. P. A. Paras, and P. A. Monson, J. Chem. Phys. **96**, 9060 (1992).
[33] C. Vega, E. P. A. Paras, and P. A. Monson, J. Chem. Phys. **97**, 8543 (1992).
[34] C. Vega and P. A. Monson, J. Chem. Phys. **107**, 2696 (1997).
[35] C. Vega, L. G. MacDowell, C. McBride, F. J. Blas, A. Galindo, and E. Sanz, J. Mol. Liq. **113**, 37 (2004).
[36] M. Marechal and M. Dijkstra, Phys. Rev. E **77**, 061405 (2008).
[37] M. Heni and H. Löwen, Phys. Rev. Lett. **85**, 3668 (2000).
[38] J. P. Hoogenboom, A. K. van Langen-Suurling, J. Romijn, and A. van Blaaderen, Phys. Rev. Lett. **90**, 138301 (2003).
[39] J. P. Hoogenboom, A. K. van Langen-Suurling, J. Romijn, and A. van Blaaderen, Phys. Rev. E **69**, 51602 (2004).
[40] T. Biben, R. Ohnesorge, and H. Löwen, Europhys. Lett. **28**, 665 (1994).
[41] M. Marechal and M. Dijkstra, Phys. Rev. E **75**, 061404 (2007).
[42] S. V. Savenko and M. Dijkstra, Phys. Rev. E **70**, 051401 (2004).
[43] M. Marechal and M. Dijkstra, Soft Matter **7**, 1397 (2011).
[44] D. Henderson, J. Quintana, and S. Sokołowski, J. Chem. Phys. **102**, 4991 (1995).
[45] A. Pressley, *Elementary Differential Geometry* (Springer Verlag, Berlin, 2010).
[46] M. Schmidt and C. von Ferber, Phys. Rev. E **64**, 051115 (2001).
[47] D. Frenkel and B. Smit, *Understanding Molecular Simulation* (Academic Press, San Diego, 2002).
[48] D. J. Tildesley and W. B. Streett, Mol. Phys. **41**, 85 (1980).
[49] Y. Rosenfeld, J. Chem. Phys. **89**, 4272 (1988).
[50] B. M. Mulder, Mol. Phys. **103**, 1411 (20 May 2005).
[51] M. Moszyńska, *Selected Topics in Convex Geometry* (Birkhäuser, Boston, 2006).
[52] I. Nezbeda, Mol. Phys. **33**, 1287 (1977).
[53] H. Hansen-Goos and R. Roth, J. Phys. Condens.: Matter. **18**, 8413 (2006).
[54] W. A. Curtin and N. W. Ashcroft, Phys. Rev. Lett. **56**, 2775 (1986).
[55] C. N. Likos, Z. T. Nemeth, and H. Lowen, J. Phys. Condens.: Matter. **6**, 10965 (1994).
[56] H. Graf and H. Löwen, Phys. Rev. E **59**, 1932 (1999).
[57] V. A. Froltsov and S. H. L. Klapp, J. Chem. Phys. **126**, 114703 (2007).
[58] B. Groh and S. Dietrich, Phys. Rev. E **63**, 021203 (2001).
[59] J. Dhont, *An Introduction to Dynamics of Colloids* (Elsevier Science, New York, 1996).
[60] M. Rex, H. H. Wensink, and H. Löwen, Phys. Rev. E **76**, 021403 (2007).
[61] M. Bier, L. Harnau, and S. Dietrich, J. Chem. Phys. **125**, 184704 (2006).
[62] L. Rossi, S. Sacanna, W. T. M. Irvine, P. M. Chaikin, D. J. Pine, and A. P. Philipse, Soft Matter **7**, 4139 (2011).
[63] A. Haji-Akbari, M. Engel, A. S. Keys, X. Zheng, R. G. Petschek, P. Palffy-Muhoray, and S. C. Glotzer, Nature (London) **462**, 773 (2009).
[64] H. H. Wensink and G. Jackson, J. Phys. Condens.: Matter. **23**, 194107 (2011).
[65] T. T. Ngo, C. M. Liddell, M. Ghebrebrhan, and J. D. Joannopoulos, Appl. Phys. Lett. **88**, 241920 (2006).
[66] N. Almarza and E. Noya, Mol. Phys. **109**, 65 (2011).
[67] F. Romano, E. Sanz, and F. Sciortino, J. Chem. Phys. **134**, 174502 (2011).
[68] Y. Xia, B. Gates, and Z. Y. Li, Adv. Mater. **13**, 409 (2001).
[69] Z.-Y. Li, J. Wang, and B.-Y. Gu, J. Phys. Soc. Jpn. **67**, 3288 (1998).
[70] A. Isihara, J. Chem. Phys. **19**, 397 (1951).
[71] R. Roth, J. Phys. Condens.: Matter. **22**, 063102 (2010).